


Phase advance constraint in K modulation for precise β -function determination

H. Garcia-Morales,^{*} M. Hofer[✉], E. H. Maclean, L. van Riesen-Haupt, and R. Tomás
CERN, 1211, Geneva 23, Switzerland

 (Received 10 February 2022; accepted 10 March 2022; published 11 April 2022)

A precise determination of the β function at different locations of an accelerator is essential to allow accurate optics correction and to ensure high machine performance. The β function can only be measured directly at locations where beam position monitors are installed. For other locations, we rely on a K -modulation technique. However, this technique presents some limitations resulting in imprecise β values when the phase advance between the modulated quadrupole and the observation point is separated by 90° . To mitigate these limitations, we have introduced the same phase advance as an additional constraint in the K -modulation algorithm. In this paper, the improvement of the β measurement uncertainty is quantified for different optics configurations for both, the LHC and the proton synchrotron (PS) booster. The new algorithm is used to reanalyze measured data during van der Meer scans for luminosity calibration providing significantly more accurate results than obtained previously. Moreover, in the PS booster, this improvement has also reduced the uncertainty of the β function at different locations of the machine.

DOI: [10.1103/PhysRevAccelBeams.25.041002](https://doi.org/10.1103/PhysRevAccelBeams.25.041002)

I. INTRODUCTION

The LHC is designed to achieve a high peak luminosity by transversely squeezing the beams at the interaction points (IPs) [1]. To achieve high luminosities, ensuring machine protection and avoiding luminosity imbalances between experiments, accurate measurements, and good control of β^* are required. The currently preferred method to determine β^* in the LHC is the K -modulation technique [2–8]. This method relies on the modulation of the gradient of the quadrupoles closest to the IP. The induced tune shifts allow a determination of the average β function at the modulated quadrupoles. The waist shift w and β^* can then be calculated via interpolation. The accuracy of the reconstructed β^* relies on the measurement uncertainty of the tune, the quadrupole gradient and positioning uncertainties, and other machine parameters. A particular case where K modulation has an important role is during van der Meer (vdM) scans in the LHC [9]. During vdM scans, the transverse separation of the two beams at the IP is scanned in both planes in order to calibrate luminosity monitors. To obtain an accurate luminosity calibration, a precise measurement of β^* is required. During 2016 vdM

scans, an optics configuration with $\beta^* = 19$ m in IP1 and IP5 was used. The measurement of β^* using K modulation provided inconsistent results in some cases [9]. These results were thought to be due to the limitations of the K -modulation algorithm. This result triggered the present study to try to overcome the limitations of the current algorithm and to extend it in order to obtain more reliable results, in particular for vdM optics. In this paper, the limitations of the K -modulation algorithm are explained as well as the new techniques implemented by adding the phase advance at the interactive region (IR) as a constraint. The new algorithm has been tested in simulations for determining β^* in different optics configurations. The data obtained during vdM scans in 2016 [9] have been reanalyzed reducing the uncertainty of the result. In order to further extend the applicability of this algorithm to other accelerators, simulations using the proton synchrotron (PS) booster lattice have been carried out showing also significant improvements in the accuracy of the measurement of the β function at locations where no diagnostic devices are available.

II. K -MODULATION TECHNIQUE

To illustrate the principle of the K -modulation technique, we focus our attention on the LHC interaction regions (IRs). However, this technique is not restricted to this example as it will be shown in the next sections. This study is particularly relevant for 90-degree phase advance lattices.

In the LHC, there are no beam position monitors (BPMs) installed at the IP, therefore, the β function at this location must be extrapolated from its measurement at a different

^{*}Also at University of Oxford, Oxford, United Kingdom.; hector.garcia.morales@cern.ch

Published by the American Physical Society under the terms of the [Creative Commons Attribution 4.0 International license](https://creativecommons.org/licenses/by/4.0/). Further distribution of this work must maintain attribution to the author(s) and the published article's title, journal citation, and DOI.

location. There exist several techniques for determining the optics function at the IP. Among them, K modulation has proven to be the preferred technique for measuring β^* [3], although this technique is not restricted to the IP and can be applied at different locations around the ring. The relationship between the variation in the quadrupole strength Δk , the average β function at the modulated quadrupole β_{av} , and the tune variation is given by

$$\beta_{av}^{x,y} = \pm \{ \cot(2\pi Q_{x,y}) [1 - \cos(2\pi \Delta Q_{x,y})] + \sin(2\pi Q_{x,y}) \} \approx \pm 4\pi \frac{\Delta Q_{x,y}}{\Delta k L}, \quad (1)$$

where $Q_{x,y}$ is the horizontal and vertical tunes and L is the length of the modulated quadrupole. From this point on, we omit the x and y subindices. The value β^* is calculated from the value of the β function at the quadrupole through the calculation of the waist position w and the β function at the waist β_w as shown in Fig. 1. The K -modulation algorithm uses Eq. (1) to estimate the average β function at the quadrupole. To simplify the following derivations, we use the thin lens approximation. The relationship between the β function at the quadrupole, β_q , and the β function at the waist position, β_w , is given by

$$\beta_q = \beta_w + \frac{(L_Q/2 + L^* - w)^2}{\beta_w}, \quad (2)$$

where L^* is the length of the last drift before the IP and $L_Q/2$ is the half length of the last quadrupole. Solving the second degree equation, we obtain

$$\beta_w^\pm = \frac{\beta_q \pm \sqrt{\beta_q^2 - 4(L_Q/2 + L^* - w)^2}}{2}, \quad (3)$$

which comprises two solutions: β_w^+ and β_w^- .

The reconstructed β_w function and waist w , given by K modulation, are related to β^* by

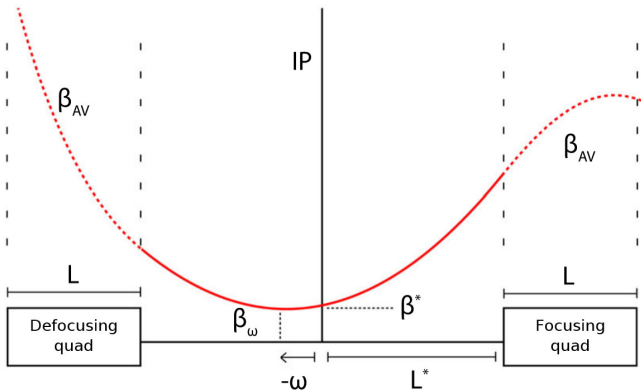


FIG. 1. Illustration of an interaction region and optics function [3].

$$\beta^* = \beta_w^\pm + \frac{w^2}{\beta_w^\pm}. \quad (4)$$

The precise derivation computing actual averages and using two quadrupoles can be found in [3]. In Eq. (4), two possible solutions are found for β^* . For low- β^* optics configurations, these two solutions are usually very far apart from each other. However, and as we will see later, for high- β^* optics configurations, the two solutions are closer and the optimization algorithm may not be sensitive enough to distinguish them.

The algorithm used to reconstruct β^* fits the measured average β function at the quadrupole for different values of the tune during the strength modulation. In addition, the results of the modulation of the two last quadrupoles in both sides of the IP are combined into a single penalty function used in the simplex optimization algorithm is given by

$$\chi^2 = \Delta\beta_{\text{foc}}^2 + \Delta\beta_{\text{def}}^2, \quad (5)$$

where β_{foc} and β_{def} are the corresponding average β functions, β_{av} at the focusing and defocusing quadrupoles, respectively, which correspond to the two quadrupoles in both sides of the IP. This approach may lead to convergence issues. In the next sections, a new penalty function is introduced in order to obtain a more accurate determination of β^* .

A. Limitations

K modulation presents some limitations in the accuracy of the reconstructed β^* , in particular for optics configurations where $\beta^* \approx L^*$, as it is the case for vdM optics configuration. By taking the derivative of Eq. (3) and assuming $w \ll L^*$, one can show that to first order the uncertainty in β^* is related to the uncertainty in β function at the modulated quadrupole as [10],

$$\frac{\sigma_{\beta^*}}{\beta^*} = \left| \frac{\partial \beta^*}{\partial \beta} \right| \frac{\sigma_{\beta_{av}}}{\beta_{av}} = \frac{\beta^* + \frac{(L^* + L_Q/2)^2}{\beta^*}}{\left| \beta^* - \frac{(L^* + L_Q/2)^2}{\beta^*} \right|} \frac{\sigma_{\beta_{av}}}{\beta_{av}} = \Lambda \frac{\sigma_{\beta_{av}}}{\beta_{av}}, \quad (6)$$

where Λ is the proportionality factor between the error in the determination of the β function at the quadrupole and the error induced in the determination of β^* . In Fig. 2, the graphical representation of Λ is shown. One can see that for $\beta^* \approx L^* + L_Q/2$, a small error in the β_{av} determination may induce a large error in β^* . This is partially compensated by introducing in the algorithm the results of the modulation of the two quadrupoles in both sides of the IP. These large errors in the determination of β^* are of particular importance for vdM optics where large β functions at the IP are used (about 19 m in IP1 and IP5) and comparable to the length of the last drift plus half of the last quadrupole length.

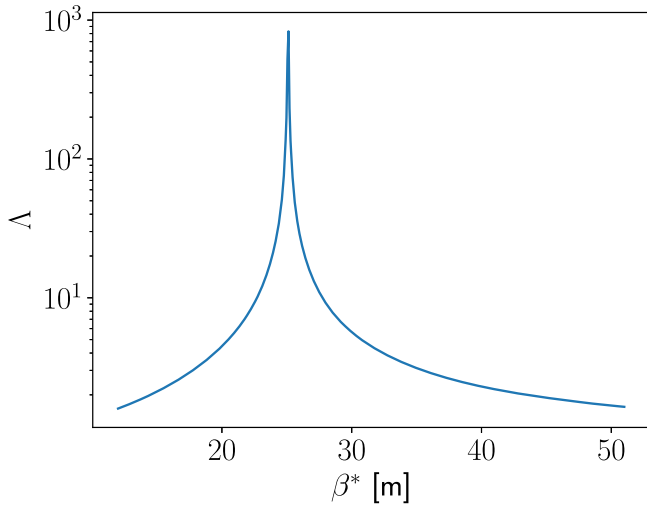


FIG. 2. Error amplification when given by Eq. (6) when $\beta^* \approx L^* + L_Q/2$. For the LHC, $L^* = 23$ m and $L_Q/2 = 2.1$ m.

A different approach to view this divergence is considering the phase advance in the IR. For $\beta^* \approx L^* + L_Q/2$, the phase advance between the IP and L^* is

$$\phi = \int_0^{L^*+L_Q/2} \frac{ds}{\beta(s)} = \int_0^{L^*+L_Q/2} \frac{ds}{\beta^* + \frac{s^2}{L^*+L_Q/2}} = \frac{\pi}{4}. \quad (7)$$

Since the β -beating wave propagates as 2ϕ , where ϕ is the IR phase advance obtained in Eq. (7), it implies that for a phase advance from the last quadrupole to the IP of $\pi/4$ (45°), the β -beating wave propagates to the IP with 90° , i.e., orthogonal to the phase value at the quadrupole.

Another limitation arises from the fact that the two solutions of Eq. (3) might be very close to each other. We can define the distance between the two solutions using

$$\Delta\beta_w = \beta_w^+ - \beta_w^- = \sqrt{\beta_{av}^2 - 4(L^* + L_Q/2 - w)^2}, \quad (8)$$

when $\beta^* \ll 1$ and the waist $w \ll L^*$, $\beta_{av}^2 \gg 4(L^* + L_Q/2 - w)^2$ and therefore, $\Delta\beta_w \gg \beta^*$. However, when β^* is comparable to L^* (i.e., for vdM optics), $\beta_{av}^2 \approx 4(L^* + L_Q/2 - w)^2$ and therefore, $\Delta\beta_w \approx 0$ and the two solutions for β_w are very close to each other. In this situation, the optimization algorithm, introduced before, may end up converging to the wrong solution (β_w^+), due to measurement uncertainties.

The trend of Eq. (8) as a function of β^* can be seen in Fig. 3 for $w = 0$. One can see that the two solutions take the same value ($\Delta\beta_w = 0$ m) when $\beta^* = L^* + L_Q/2$, as it was found in Eq. (6). In particular, and always assuming that the waist w is small compared to L^* , for $\beta^* = \beta_w^- = 30$ cm, the average β function at the quadrupole is $\beta_{av} = 1763$ m and thus, the second solution is, $\beta_w^+ = \beta^* + \Delta\beta_w \approx \Delta\beta_w = 1763$ m. Therefore, in this case, it is highly improbable that the

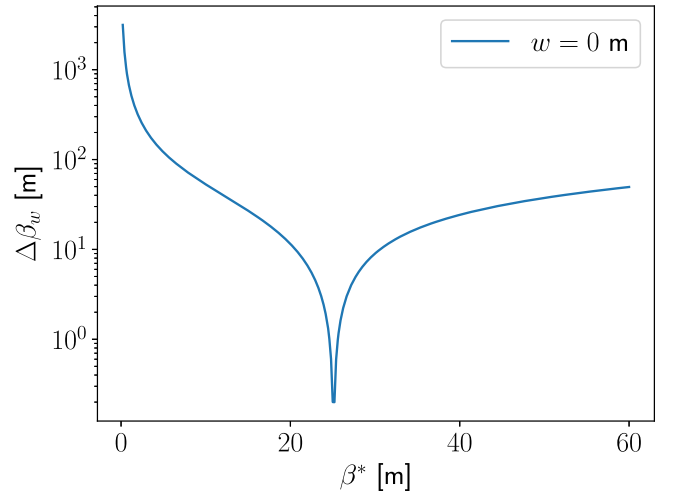


FIG. 3. Difference between the two solutions given by Eq. (8) as a function of β^* .

algorithm converges to the β_w^+ solution. However, for $\beta^* = 19$ m, resulting in an average β function at the quadrupole, $\beta_{av} \approx 46.84$ m. This gives a difference between the two solutions of only $\Delta\beta_w \approx 9$ m. In this case, the probability for the algorithm to converge to the wrong solution (β_w^+) is not negligible. This paper presents an improvement of the K -modulation technique to overcome these limitations by adding new constraints.

III. K MODULATION FOR DIFFERENT OPTICS CONFIGURATIONS

K -modulation simulations were performed using MAD-X code [11] to extend the study to ten different optics configurations with different β^* from 12 to 50 m. Systematic errors were introduced, namely a magnet

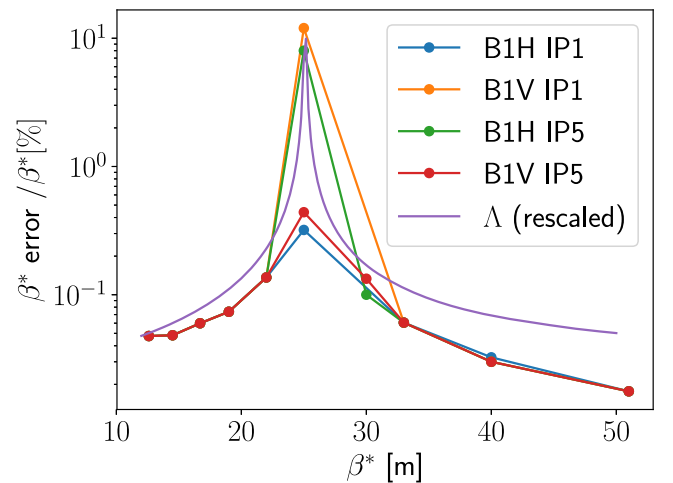


FIG. 4. Relative error in β^* extracted from simulations as a function of the selected optics and a tune uncertainty $\delta Q = 5 \times 10^{-5}$. We can see that for $\beta^* \sim L^* + L_Q/2$, the relative error in β^* increases significantly.

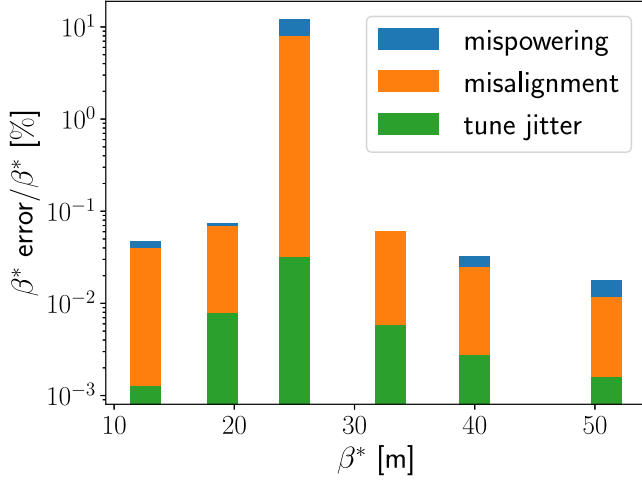


FIG. 5. Contribution of different errors to the total error in the β^* determination from K modulation for B1 vertical plane in IP1 for different optics configurations.

misalignment of 6 mm and a magnet strength error of $\Delta K/K = 10^{-3}$. We evaluate the error in the β^* determination as a function of the selected β^* for the case of a tune uncertainty of $\delta Q = 5.0 \times 10^{-5}$. The value for $\Delta\beta^*/\beta^*$ is obtained by comparing the error in β^* obtained from K modulation with the reference β^* . As it can be seen in Fig. 4, for $\beta^* = 25$ m, the error diverges while the error decreases when β^* is larger or smaller. The maximum relative deviation occurs at exactly the same location predicted above and shown in Fig. 2. In Fig. 5, the contribution from different errors is shown for the horizontal plane in IP1 for B1. This was obtained by simulating the different sources of errors separately. In all optics configurations, misalignment seems to have a larger impact on the error of β^* .

IV. CONSTRAINING K -MODULATION SOLUTIONS USING IR PHASE ADVANCE

The penalty function shown in Eq. (5) only takes into account the average β functions at the quadrupoles. If an additional term, taking into account another observable, is added, the solution can be further constrained and the uncertainty in β^* is reduced. In particular, the phase advance in the IR plays an important role in the determination of β^* . For that reason, the measured phase advance at the IR using an ac dipole is introduced when available. To measure the IR phase advance, the ac dipole is used to generate a transverse excitation. By means of harmonic analysis on the recorded BPM signal, we can extract the phase advance between the two adjacent BPMs in both sides of the IP. The phase advance ϕ_{IP} along the drift that contains the IP can be evaluated as [12]

$$\phi_{\text{IR}} = \arctan\left(\frac{\hat{L}^* - w}{\beta_w}\right) + \arctan\left(\frac{\hat{L}^* + w}{\beta_w}\right), \quad (9)$$

where \hat{L}^* is the distance between the IP and the closest BPM. From Eq. (9), we can calculate the phase advance using the reconstructed β_w and w . This value is compared to the reference value obtained from the measurement of the phase advance. The figure of merit χ^2 from Eq. (5) can be extended to include the additional phase advance constraint,

$$\chi^2 = (1 - \Omega) \left[\left(\frac{\Delta\beta_{\text{foc}}}{\beta_{\text{foc}}} \right)^2 + \left(\frac{\Delta\beta_{\text{def}}}{\beta_{\text{def}}} \right)^2 \right] + \Omega \left(\frac{\Delta\phi_{\text{IR}}}{\phi_{\text{IR}}} \right)^2. \quad (10)$$

In order to account for the different magnitudes of the change in β and ϕ , the different terms have been normalized to their design parameters. In such a way, the algorithm tries to reduce $\Delta\beta$ and $\Delta\phi$ independently of the actual values of these parameters. The contributions in Eq. (10) are weighted and the weight can be adjusted manually in order to give higher preference to the phase or to the β -function value at the quadrupole location. In the next section, we present more details about the impact of the value of Ω for different optics configurations.

V. SIMULATIONS

In this section, the phase advance constraint has been tested to evaluate its impact in different optics configurations. Since we expect significant differences between different optics, two different regimes have been tested: high- β^* and low- β^* optics configurations.

A. High- β^* optics

For vdM scans, an optics configuration with $\beta^* = 19.2$ m is used to perform simulations of K modulation. Systematic errors in the quadrupole magnetic fields distributed according to Table I [13], 6 mm longitudinal misalignment of the quadrupoles randomly assigned and a tune uncertainty of $\delta Q = 5 \times 10^{-5}$ are included in the simulations. A total of 500 seeds were simulated with errors randomly assigned to the different quadrupoles. The spread in β^* and IR phase ϕ_{IR} from the model before simulating K -mod techniques are shown in Fig. 6. This gives the reference of the spread in β^* . The standard deviation of this distribution is about 1 m in both planes. This reflects the initial statistical uncertainty we expect before the measurement. Among these 500 seeds, and after applying

TABLE I. Magnetic errors used in different quadrupoles taking [13] as a reference with a larger relative error in MQX.

Quadrupole	Relative error (10^{-4})
MQ	17
MQM	12
MQY	7
MQX	7
MQW	13
MQT	77

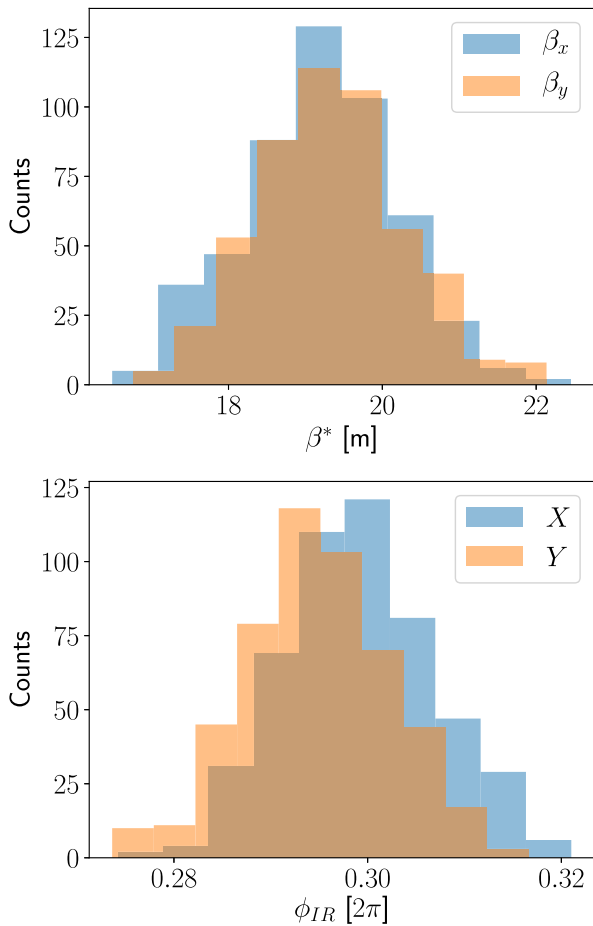


FIG. 6. Histograms for β^* beating and ϕ_{IR} extracted from the model after introducing magnetic errors in the quadrupoles for IP1 before K modulation is applied.

K modulation, some of them converged to the wrong solution for β^* as explained in previous sections. For one of these seeds, we have scanned the value of waist w and the β function at this location, β_w , and the figure of merit χ^2 from Eq. (10) was evaluated in each case for different values of the weight Ω . We can see in the top plot of Fig. 7 that when the phase advance is not included as a constraint (top plot, $\Omega = 0$), the algorithm converges to the secondary minimum. When the phase constraint is included (middle plot, $\Omega = 0.1$) using a realistic model of the machine that mimics the actual phase measurement, the secondary minimum disappears and the algorithm converges to the only minimum available which corresponds to the expected solution. If the weight Ω is further increased, any remainder of the secondary minimum is removed and the convergence to the primary minimum is ensured. In addition, the uncertainty of the waist w is not affected as it can be seen in Fig. 8.

The actual value of Ω that removes the secondary minimum depends on the particular combination of errors in the machine. Therefore, its value must be chosen large enough to ensure that there are no cases where the

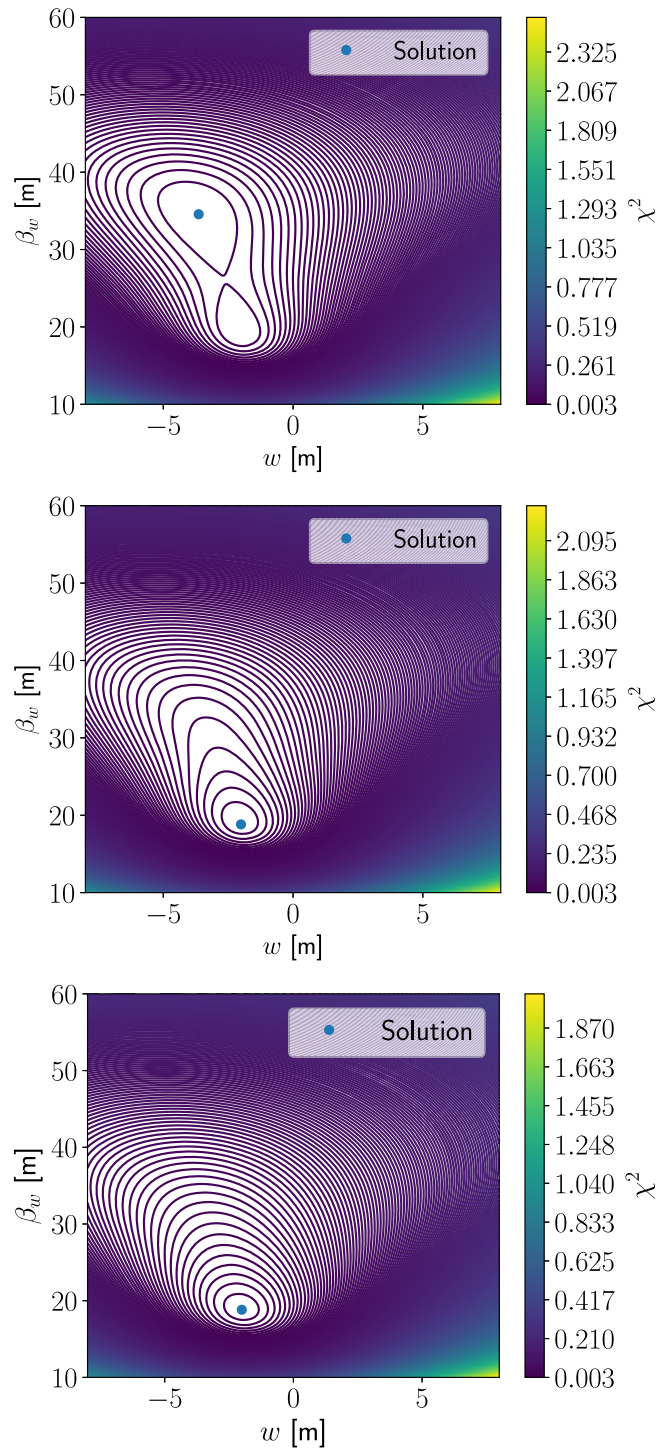


FIG. 7. Example of how the optimization algorithm can converge to the wrong solution (top) and how the introduction of the phase advance constraint [$\Omega = 0.1$ (middle) and $\Omega = 0.2$ (bottom)] helps in finding the real minimum for the case of vdM optics configuration.

algorithm converges to the nonoptimal solution. In Fig. 9 (top), the relative number of seeds converging to the right minimum is shown as a function of the weight Ω . First, we can see that for low values of Ω , the number of

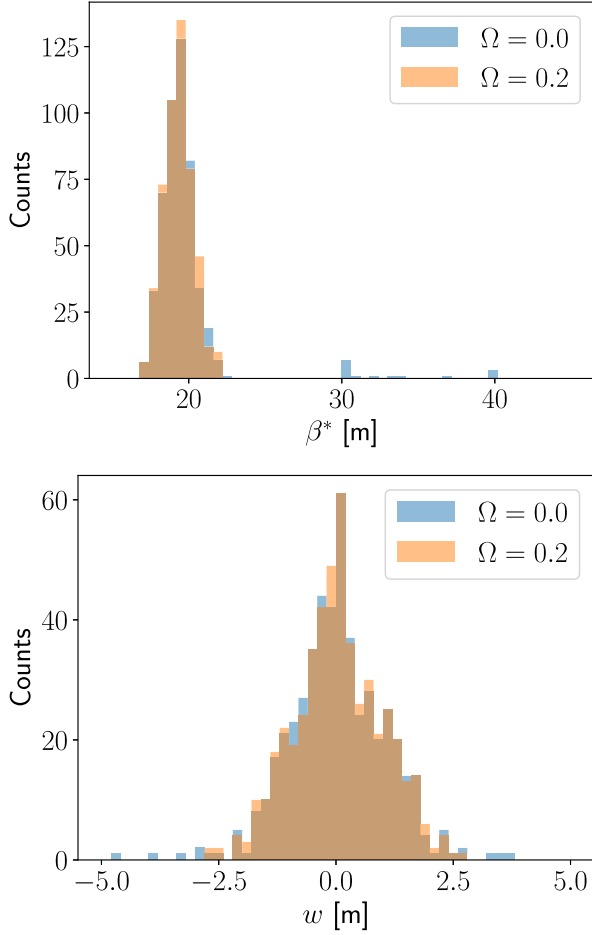


FIG. 8. Histogram of the reconstructed vertical β^* (top) and vertical waist (bottom) w using K modulation in IP1 for different values of the weight Ω .

seeds that fail to converge to the right minimum is above 5%. We observe that all seeds converge correctly already for $\Omega = 0.07$. However, since the phase advance between BPMs in both sides of the IP does not provide information about the waist, we risk reducing the uncertainty of the reconstructed w . Nevertheless, we have seen that very high values of Ω are required to affect negatively the uncertainty of the waist w . Therefore, we have taken a more conservative approach by choosing $\Omega = 0.2$ as the default value to ensure a right convergence for all seeds. In addition, in Fig. 9 (bottom), the error in the reconstructed β^* using K modulation as a function of Ω is shown. Initially, for $\Omega = 0$, the uncertainty goes beyond 12%. When the weight Ω is increased, the uncertainty is reduced to less than 0.7%. Hence, we conclude that, when we constrain the solution with the phase advance, the uncertainty of the reconstructed β^* using K modulation is also reduced significantly.

Taking into account all 500 seeds, the average reconstructed β^* is shown in Table II including its deviation from the value obtained from the perturbed model.

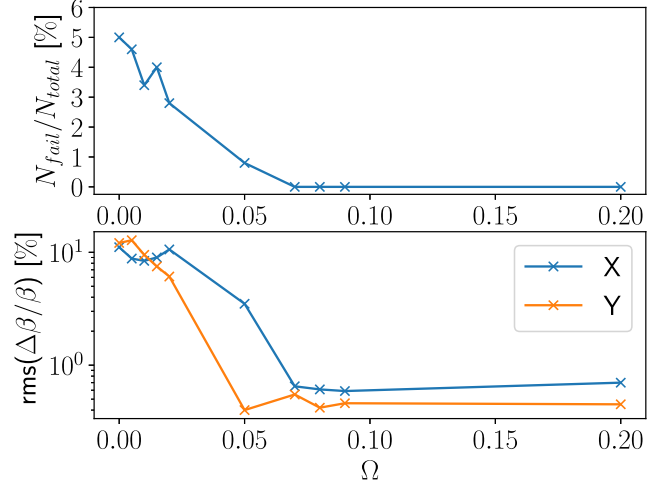


FIG. 9. Fraction of the reconstructed β^* values using K modulation that converges to the wrong solution (top) and statistical uncertainty of the measurements (bottom).

The uncertainty in β^* is reduced by more than a factor of 10 when the phase constraint is taken into account. For values of the weight Ω larger than 0.2, the uncertainty of β^* is not further reduced. This example demonstrates that the addition of the IR phase constraint greatly improves the performance of the K -modulation algorithm for high- β^* configurations.

B. Injection optics

We consider now the case of LHC injection optics with $\beta^* = 11$ m in IP1 and IP5. This case is of particular interest since the corrections of the optics at injection require special dedication and the value of β^* is still high. The LHC injection optics accommodates the beam coming from the super PS during the filling process. Once the machine is full, the energy ramp starts and the optics is smoothly adapted accordingly. One of the recent improvements is to start squeezing the beams at the IPs already during the ramp, the so-called ramp and squeeze. Since the optics is changed discretely, one has to ensure that at each step the optics are properly corrected. For that reason, a good knowledge of the optics at each step is crucial to ensure that the full process of ramp and squeeze is completed.

We have performed K -modulation simulations to reconstruct β^* using the phase advance as a constraint using the

TABLE II. Reconstructed average and uncertainty of β^* and waist from K modulation for $\beta^* = 19$ m optics configuration.

Ω	β_x^* [m]	rms ($\Delta\beta_x^*/\beta_x^*$) [%]	β_y^* [m]	rms ($\Delta\beta_y^*/\beta_y^*$) [%]
0.0	19.5	11.1	19.7	12.1
0.1	19.2	0.6	19.3	0.5
0.2	19.2	0.7	19.3	0.4

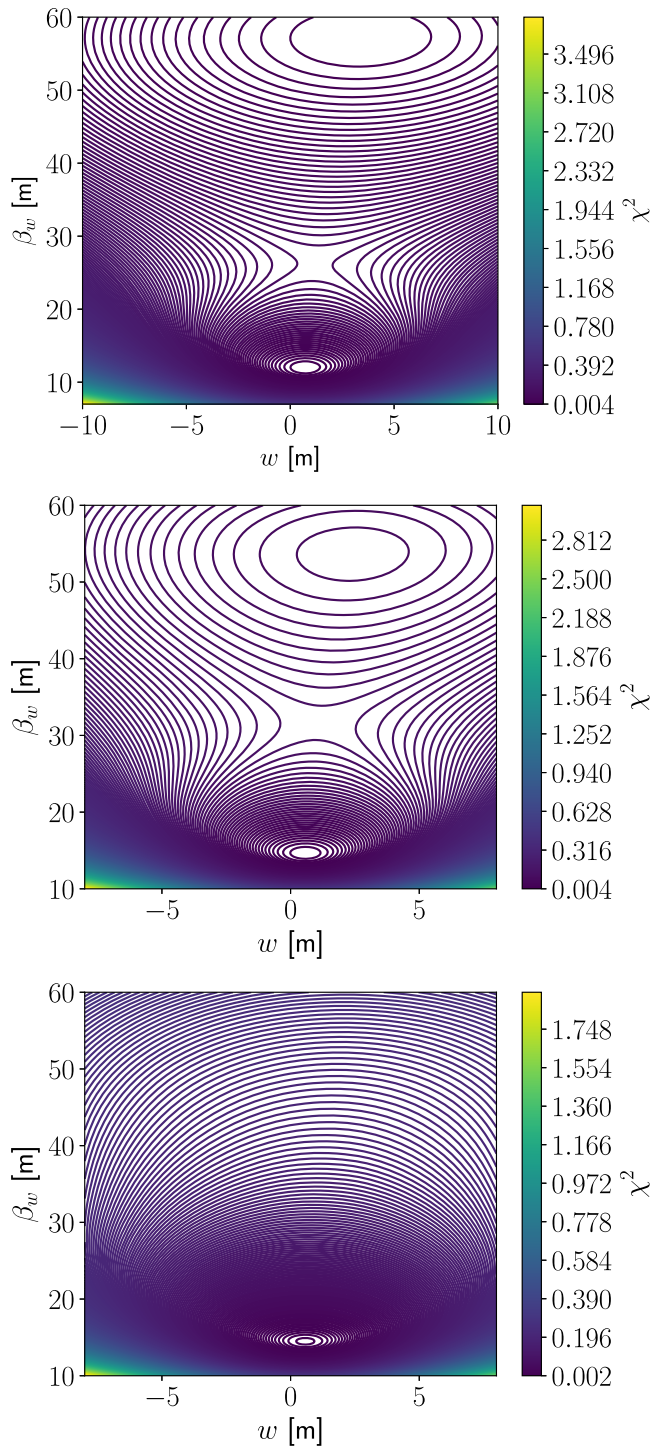


FIG. 10. Scans over w and β_w and the figure of merit value obtained for different phase advance weights: $\Omega = 0$ (top), $\Omega = 0.2$ (middle), and $\Omega = 0.5$ (bottom) for LHC injection optics.

regular LHC injection optics. In Fig. 10, the results of the waist w and β_w scans are shown for different values of the weight Ω . We can see that in this case, the weight Ω must be chosen $\Omega = 0.5$ in order to remove the minimum that drives to the second and nonoptimal solution. One can also see

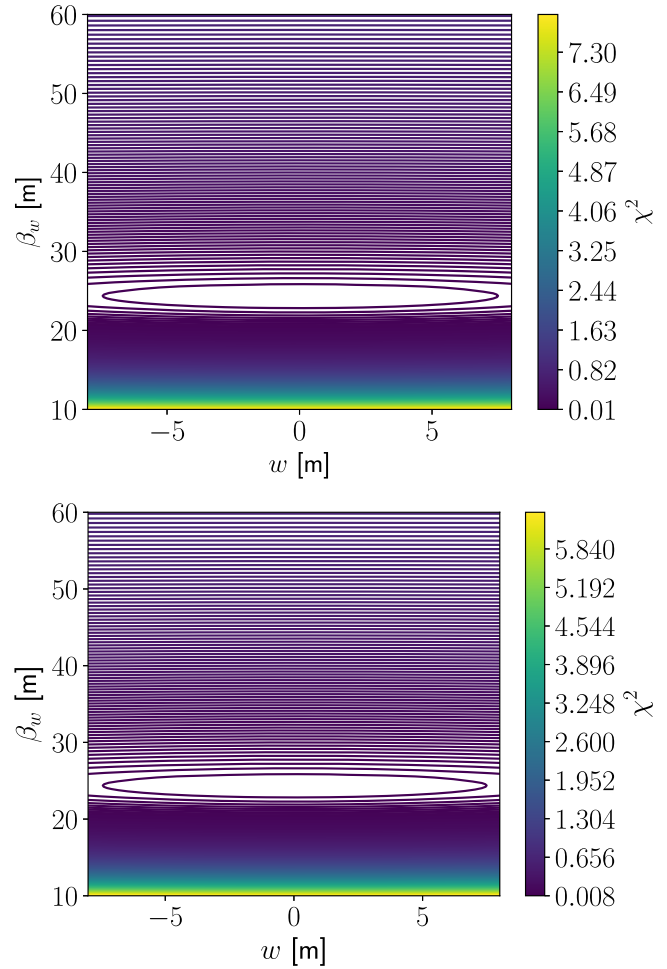


FIG. 11. Example of the optimization algorithm for low- β^* for $\Omega = 0$ (top) and $\Omega = 0.2$ (bottom). Regardless of the value of the weight, Ω will always converge the right solution.

that the island corresponding to the nonoptimal solution covers a larger area than for $\beta^* = 19$ m. This means that, even if this local minimum is higher than the real minimum, the probability of falling in this area is significantly high. For that reason, it is recommended to use the phase constraint to remove the secondary minimum and ensure that the algorithm converges to the right solution.

C. Low- β^* optics

The impact of the implementation of the IR phase advance to constrain the K -modulation solutions has also been tested for low- β^* optics configurations. In particular, we have used LHC optics with $\beta^* = 30$ cm in IP1 and IP5. In that case, we expect the algorithm to always converge to the optimal solution even without including the phase advance in the IR as a constraint. As it was shown analytically, this is due to the fact that the two solutions coming from Eq. (3) are initially very far apart from each other. As it is seen in Fig. 11, the effect of increasing the phase weight Ω would not significantly modify the

TABLE III. Reconstructed average and uncertainty of β^* from K modulation for $\beta^* = 30$ cm optics configuration.

Ω	β_x^* [cm]	rms ($\Delta\beta_x^*/\beta_x^*$) [%]	β_y^* [cm]	rms ($\Delta\beta_y^*/\beta_y^*$) [%]
0.0	33.8	6	34.0	8
0.1	33.8	6	34.0	8
0.2	33.8	6	34.0	8

topology of the result and, therefore, it has little impact on the convergence dynamics of the optimization algorithm.

Taking into account all 500 simulated seeds, the reconstructed values for β^* and its deviation from the value obtained with the perturbed model are shown in Table III. We can see that the relative deviations of β^* are always below 10%, which is the estimated value found for HL-LHC in [3] for a 33-cm optics configuration and the same tune uncertainty of 5×10^{-5} . Note that to meet the tight β^* control requirements in HL-LHC, a tune uncertainty of about 2×10^{-5} would be needed or a combination of different measurement techniques [12]. As expected from the above analytical derivations, the impact of the phase advance constraint in K modulation for low- β^* optics is negligible.

VI. MEASUREMENTS USING VDM OPTICS

Data from a dedicated machine development (MD) session that was carried out in 2016 for vdM optics measurement are reanalyzed taking into account the improvements in the algorithm presented above. In total, eight quadrupole modulations were performed, one per side of IP1 and IP5 and two on either side of IP8 with and without orbit feedback activated. It is important to quantify

TABLE IV. Tune uncertainties during the MD carried out for vdM optics measurements.

	$\delta Q_x [10^{-5}]$	$\delta Q_y [10^{-5}]$
B1	3.2	3.2
B2	2.3	3.4

the uncertainty on the tune measurement itself since it contributes to the total error in the reconstruction of β^* . The uncertainty of the tune measurement is evaluated during a 5 min period before the start of the quadrupole modulation. In Table IV, the measured tune uncertainty in each case is shown. Nevertheless, for both measurements and simulations, a slightly more pessimistic scenario has been considered and a tune uncertainty of 5×10^{-5} was used. Other systematic errors were introduced, namely magnet misalignment of 6 mm and magnet strength errors of $\Delta K/K = 10^{-3}$.

Previous analyses reported in [9] revealed that, in some cases, when the phase advance is not included to constrain the solution of the β^* , the algorithm was not able to converge to the right solution. These large deviations can be partially mitigated by introducing the measured IR phase advance to constrain the solution. In Table V, the measured phase advances in the IR using the ac dipole to constrain the K -modulation solution are shown. In Table VII, the reconstructed β^* at the different IPs is shown for a phase weight of $\Omega = 0.2$. This table can be compared with the same analysis performed with $\Omega = 0$ VI. We can see that now the results are closer to the expected values and the uncertainties have been reduced significantly. Therefore, beyond the tests performed in simulations, we see that the

TABLE V. Measured phase advance and standard deviation (in 2π units) in IR1, IR5, and IR8 during the 2016 MD on vdM optics.

IP	Beam 1				Beam 2			
	ϕ_x	$\sigma_{\phi_x} [10^{-4}]$	ϕ_y	$\sigma_{\phi_y} [10^{-4}]$	ϕ_x	$\sigma_{\phi_x} [10^{-4}]$	ϕ_x	$\sigma_{\phi_y} [10^{-4}]$
1	0.2595	5	0.2606	3	0.2873	7	0.2633	5
5	0.2660	6	0.2775	3	0.2750	4	0.2593	6
8	0.2389	7	0.2342	7	0.2422	6	0.2233	4

TABLE VI. Measured β^* and its associated error in IP1, IP5, and IP8 using K mod during the 2016 MD on vdM optics after introducing the IR phase advance as a constraint with $\Omega = 0$.

IP	Beam 1					Beam 2				
	β_{nom}^* [m]	β_x^* [m]	$\frac{\Delta\beta_x^*}{\beta_x^*}$ [%]	β_y^* [m]	$\frac{\Delta\beta_y^*}{\beta_y^*}$ [%]	β_x^* [m]	$\frac{\Delta\beta_x^*}{\beta_x^*}$ [%]	β_y^* [m]	$\frac{\Delta\beta_y^*}{\beta_y^*}$ [%]	
1	19.2	17.40	5.7	18.12	0.5	17.70	1.0	17.37	0.4	
5	19.2	20.87	0.6	19.59	0.4	16.19	0.2	18.59	0.4	
8	24	21.49	0.7	20.00	0.5	26.36	0.04	22	70	

TABLE VII. Measured β^* and its associated error in IP1, IP5, and IP8 using K mod during the 2016 MD on vdM optics after introducing the IR phase advance as a constraint with $\Omega = 0.2$.

IP	Beam 1					Beam 2			
	β_{nom}^* [m]	β_x^* [m]	$\frac{\Delta\beta_x^*}{\beta_x^*}$ [%]	β_y^* [m]	$\frac{\Delta\beta_y^*}{\beta_y^*}$ [%]	β_x^* [m]	$\frac{\Delta\beta_x^*}{\beta_x^*}$ [%]	β_y^* [m]	$\frac{\Delta\beta_y^*}{\beta_y^*}$ [%]
1	19.2	18.7	2.1	18.73	0.4	17.58	0.4	17.96	0.4
5	19.2	20.30	0.3	19.18	0.3	16.56	0.5	19.15	0.3
8	24	22.63	0.5	22.41	0.5	19.6	3.3	18.90	0.2

improvements introduced in the algorithm to find β^* also have a significant impact on the measurements. These improvements allow to obtain a new set of reference values for β^* during vdM optics scans. Table VII can be used as a reference for run 2 studies on luminosity calibration in the experiments. In future vdM scans during run 3, this new methodology will be applied in order to precisely calibrate luminosity.

VII. APPLICATION TO PS BOOSTER

In the preceding sections, it was shown that divergent uncertainty on the extrapolation of β functions to experimental IPs in the LHC represented a serious challenge to the successful operation of that machine. The divergence was associated with optics conditions wherein $\beta^* \approx L^*$. Such a limitation was shown to be overcome through modification of the standard method of K -mod extrapolation, to include an additional constraint based on measurement of the phase advance across the insertion.

In practice, similar limitations on the application of K modulation arise in various machines. A clear example of this can be seen in the PS booster at CERN. The PS booster is a 25 m radius synchrotron accelerating protons in four stacked rings from the kinetic energy of 160 MeV to 2.0 GeV. It directly serves the Isotope mass Separator On-Line facility (ISOLDE) experiment at CERN, as well as serving as the first synchrotron in the CERN injector chain. As such, it represents a very different machine configuration to the LHC.

Precise emittance measurement is of particular interest to PS booster operation, which requires an accurate knowledge of the β functions at the location of the wire scanners (BWS). The PS booster operates at integer tunes of $Q_{\text{int}} = 4$ in both planes, with a $\Delta\phi \approx 90^\circ$ phase advance between BPMs. Consequently, the capability of turn-by-turn optics methods is extremely limited. Figure 12 shows the MAD-X layout and optics of the PS booster in the vicinity of a PS booster wire scanner (this layout is representative of all BWS locations).

Minimal space is available in the PS booster for addition of extra BPMs close to the wire scanner. Consequently, K modulation of the focusing quadrupoles (QFO) on either side of the wire scanner, followed by extrapolation of the measured β_{QFO} to the wire scanner location, would be of significant interest. In practice, the PS booster operates very

close to the divergent condition on Λ [outlined in Eq. (6)] in the wire scanner insertion, particularly in the vertical plane. This is illustrated in Fig. 13, which shows extrapolated uncertainty via Eq. (6) for several σ_β/β . Depending on the specific operational scenario and β beating, the PS booster can move closer or further from the divergent condition.

To assess the viability of K modulation, extrapolation was attempted in simulations from the focusing quadrupoles on either side of the wire scanner. About 1000 instances of the PS booster model were considered, encompassing the operational range of working points. For the purpose of testing, a constant 0.05% error was taken on the average β function in the quads. The extrapolation was then performed with perfect machine knowledge (the extrapolation was performed using the same Polymorphic

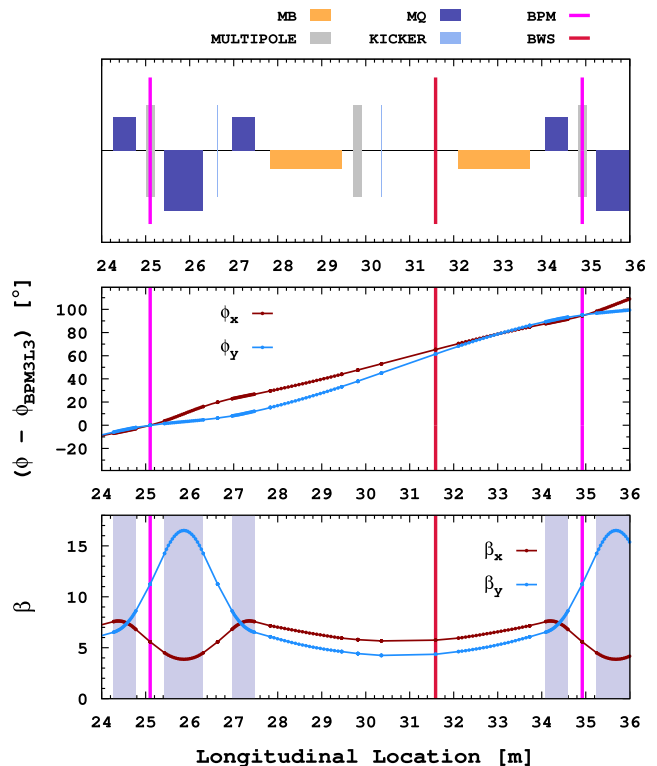


FIG. 12. MAD-X layout of the PS booster lattice in the vicinity of wire scanner (top) together with simulated phase advance (center) and β functions (bottom). The wire scanner location is indicated by a red line.

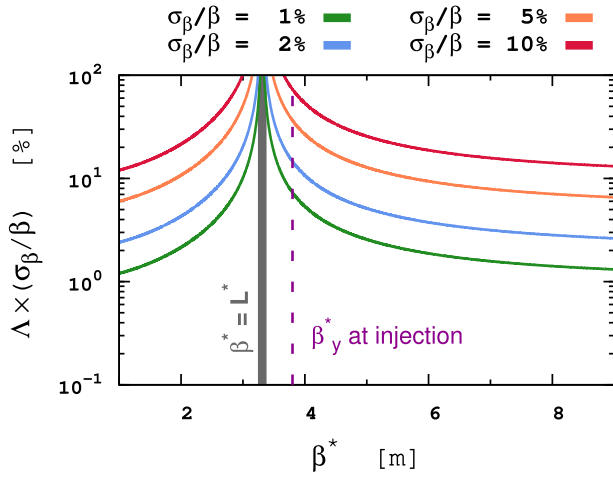


FIG. 13. Analytical uncertainty on extrapolated β , as determined by Eq. (6), from the PS booster QFO in the wirescanner insertions.

Tracking Code model as defined for the test case). Results from the standard K-mod constraint, Eq. (5), are shown in Fig. 14 (orange).

Up to 40% errors were obtained on the inferred β at the wirescanner, even for an unrealistically small error on the average β at the quadrupoles. Clearly, the standard K-mod extrapolation (Fig. 14, orange) does not represent a viable option to determine β at the wirescanners.

A similar analysis was performed using the modified K-mod extrapolation technique outlined in the preceding sections, via optimization of Eq. (10). The phase advance between the closest BPMs to the wirescanner (shown in Fig. 12, pink) provided the additional constraint, and a weighting of $\Omega = 0.3$ on the phase constraint was employed, this having shown positive results for the LHC studies presented previously. Results for 1000 test cases with the modified extrapolation technique are shown in Fig. 14 (black). In this case, an excellent agreement between the true and inferred β at the wirescanners was obtained.

Data shown in Fig. 14 (black) correspond to an unrealistically good measurement quality for the K modulation but demonstrates in principle that using the refined extrapolation constraint allows measurement of the optics at the PS booster wirescanners. A further scenario was considered, where realistic measurement uncertainties were introduced into the test cases. Measurement errors were added to the average β at the quadrupoles with a Gaussian distribution of $\sigma_{\beta, \text{avg}} = 2\%$, truncated at 3σ . Gaussian longitudinal alignment errors with $\sigma_s = 0.5$ cm, truncated at 3σ were applied. Errors on the quadrupole strength used to define average β at the quads during optimization were taken to have $\sigma_{\beta, \text{avg}} = 0.5\%$, truncated at 3σ . A measurement error on the inter-BPM phase advance used in the extrapolation constraint was applied with $\sigma_\phi = 2\pi \times (5 \times 10^{-4})$, truncated at 3σ . Results for 1000 test cases including these measurement errors are shown in Fig. 15 (light blue). A histogram of the

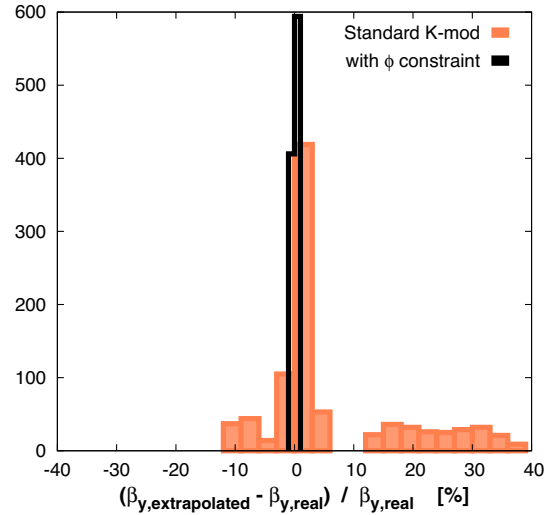


FIG. 14. Histograms of the percentage error on the β_y at the location of the PS booster wirescanner, as determined in simulation via extrapolation from the nearest quadrupoles. Results are shown for 1000 test cases of the PS booster model encompassing the operational range of working points. Results are shown for the standard K-mod extrapolation method via minimization of Eq. (5) (orange) and for the K-mod extrapolation including the phase constraint, Eq. (10), with $\Omega = 0.3$ (black).

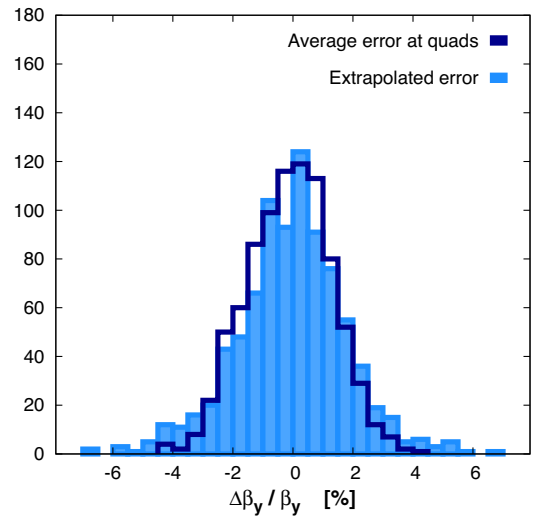


FIG. 15. Histograms of the percentage error on the β_y at the location of the PS booster wirescanner, as determined in simulation via extrapolation from the nearest quadrupoles, including constraint on the phase advance of the closest BPMs. Results are shown for 1000 test cases of the PS booster model encompassing the operational range of working points and including a range of realistic measurement errors (light blue). A histogram of the applied test-case error on the average β at the modulated quadrupoles is shown in dark blue. The value given is the mean of the error introduced to the left and right quadrupoles.

applied error added to the average β at the quadrupoles is also shown in dark blue (where the mean error between the left and right quads is indicated).

A maximum deviation of 7% was obtained for the inferred β_{BWS} from the true value. This is comparable to the applied distribution of errors on the average β at the quadrupoles. Given a sufficient quality of K -modulation measurement at the quadrupoles therefore, extrapolation of the measurement to the PS booster wirescanner appears viable using the method outlined in this paper. Consequently, investigation of the hardware upgrades necessary to facilitate independent modulation of the nearby quadrupoles is ongoing in the PS booster.

VIII. CONCLUSIONS

K modulation is the most accurate technique to determine β function at the IPs of the LHC. Nevertheless, it presents a significant limitation when the phase advance between the modulated quadrupole and the observation location is separated by 90-degree phase advance.

This is reflected in van der Meer optics in the LHC, where β^* is comparable to L^* . We have shown that introducing the measured phase advance in the IR to further constrain the K -modulation β^* , we can avoid this limitation and improve the uncertainty of the reconstructed β^* . In particular, it has a significant impact when high- β^* optics is considered as it is the case for the optics configuration used during vdM scans. It could be also beneficial if β^* is also measured at injection which might be the case during run 3.

Profiting from this development, a new analysis on data obtained using K modulation for β^* determination during vdM scans was carried out and new reference values for β^* at different IPs were obtained. This information is essential for a precise luminosity calibration in the experiments. This new methodology will be also fundamental for future studies that require precise measurements of β^* during run 3 and the HL-LHC.

The analysis was extended to the PS booster showing also significant improvements on the determination of the β function. This last result demonstrates that this new algorithm can be further extended to any other machine, in particular when the phase advance between the modulated quadrupole and the BPM is 90°.

ACKNOWLEDGMENTS

The authors are really grateful to Gianluigi Arduini and Paul Collier for their comments, which significantly improved the quality of the manuscript. This work was supported by a HL-LHC UK STFC grant.

- [1] L. Evans and P. Bryant, LHC machine, *J. Instrum.* **3**, S08001 (2008).
- [2] M. G. Minty and F. Zimmermann, *Measurement and Control of Charged Particle Beams* (Springer-Verlag, Berlin, 2003), pp. 30–32.
- [3] F. Carlier and R. Tomás, Accuracy and feasibility of the β^* measurement for LHC and high luminosity LHC using k -modulation, *Phys. Rev. Accel. Beams* **20**, 011005 (2017).
- [4] M. Hofer, F. Carlier, and R. Tomás, K -modulation in future high energy colliders, in *Proceedings of the 10th International Particle Accelerator Conference (IPAC-2019), Melbourne, Australia, 2019* (JACoW, Geneva, Switzerland, 2019), MOPMP022, pp. 476–479.
- [5] P. Thrane, R. Tomás, A. Koval, K. Ohmi, Y. Ohnishi, and A. Wegscheider, Measuring β^* in SuperKEKB with K modulation, *Phys. Rev. Accel. Beams* **23**, 012803 (2020).
- [6] J. Cardona, Y. Rodríguez, and R. Tomás, A twelve-quadrupole correction for the interaction regions of high-energy accelerators, [arXiv:2002.05836](https://arxiv.org/abs/2002.05836).
- [7] T. Persson, F. Carlier, J. Coello de Portugal, A. Garcia-Tabares Valdivieso, A. Langner, E. H. Maclean, L. Malina, P. Skowronski, B. Salvant, R. Tomas, and A. C. Garcia Bonilla, LHC optics commissioning: A journey towards 1% optics control, *Phys. Rev. Accel. Beams* **20**, 061002 (2017).
- [8] C. A. Lindström, R. D’Arcy M. J. Garland, P. Gonzalez, B. Schmidt, S. Schröder, S. Wesch, and J. Osterhoff, Matching small β functions using centroid jitter and two beam position monitors, *Phys. Rev. Accel. Beams* **23**, 052802 (2020).
- [9] R. Alemany-Fernández *et al.*, Cross-calibration of the LHC transverse beam-profile monitors, in *Proceedings of the 8th International Particle Accelerator Conference (IPAC-2017), Copenhagen, Denmark, 2017* (JACoW, Geneva, Switzerland, 2017), MOPAB130, pp. 437–440.
- [10] L. van Riesen-Haupt, J. M. Coello de Portugal, E. Fol, A. Seryi, and R. Tomás, K -modulation developments via simultaneous beam based alignment in the LHC, in Ref. [9], TUPVA042, pp. 2159–2162.
- [11] CERN-BE/ABP Accelerator Beam Physics Group, Methodological accelerator design (MADX), <http://mad.web.cern.ch/mad>.
- [12] J. Coello-de-Portugal, R. Tomás, and M. Hofer, New local optics measurements and correction techniques for the LHC and its luminosity upgrade, *Phys. Rev. Accel. Beams* **23**, 041001 (2020).
- [13] A. Langner and R. Tomás, Optics measurement algorithm and error analysis for the proton energy frontier, *Phys. Rev. ST Accel. Beams* **18**, 031002 (2015).